# Influence of Forebody Cross-Sectional Shape on Wing Vortex-Burst Location

Robert M. Hall*
*NASA Langley Research Center, Hampton, Virginia*

**A water-tunnel study examining the influence of forebody cross section on the position of the wing vortex burst was carried out in the NASA Ames-Dryden water tunnel for a 55-deg cropped delta-wing model. Two of three cross sections investigated were chine-shaped, where the included angle of the chine was either 7.5-deg, representing a rather small side-edge angle, or 90-deg, representing a more moderate design. The third cross section was circular and served as a baseline for comparison. It is found that the 7.5-deg chine cross section generated the strongest forebody vortices of the three configurations and that these strong forebody vortices interacted with the main wing vortices in such a manner as to dramatically delay wing vortex-burst position at zero sideslip. If the configuration is sideslipped, large asymmetries in wing vortex burst location may result.**

## Nomenclature

$c$ = wing chord as measured along wing/fuselage junction, 7.5 in.
$x$ = longitudinal distance forward of wing trailing edge/fuselage junction, in.
$y$ = lateral dimension from center of fuselage, in.
$z$ = distance above plane formed by chine edges, in.
$\alpha$ = angle of attack, deg
$\beta$ = angle of sideslip, deg
junc = junction

## Introduction

As modern fighter aircraft are expected to maneuver to ever higher angles of attack,[1-3] increasing demands are placed on the aircraft designer to account for the intense vortex flow often generated on the leeward side of the aircraft forebody. This vortex generation can result in difficulties such as a destabilizing pitchup tendency or large forebody side forces stemming from asymmetric vortex shedding. Understanding the isolated forebody flow, which is still a challenge,[4-7] is only a part of the problem. An additional challenge is to account for the interaction between the possibly strong forebody vortices and vortices generated by sharp-edged delta wings.

Whereas most of the analytic and experimental work addressing the forebody problem has employed circular cross sections, other classes of cross sections may be of interest to the forebody designer. One such class is cross sections with sharp edges, or chine-shaped cross sections. The present generic study was undertaken to test two different cross sections with sharp edges and compare their characteristics to a circular fuselage having the same planform, with particular emphasis on the vortex-burst phenomenon.

## Experimental Details

### Water-Tunnel Description

The tests were performed in the Ames-Dryden water tunnel, shown in Fig. 1. The tunnel is 15 ft high, 24 ft long, and 2 ft wide. The test section measures 24 × 16 in. and is 72 in. long. The configurations were installed so that the wing plane is parallel to the 16-in. side at $\alpha = 0$ deg. The walls of the test section are constructed of 2-in.-thick Plexiglas, which permits a 360-deg view of the test in progress. The test section has a door on its side for easy access to the model and sting. The velocity range of the water tunnel can be varied from 0.05 to 1.1 ft/s but is typically run at 0.25 ft/s. At this flow rate, the mean velocity profile remains within 1% of the centerline velocity over the majority of the test section with a turbulence level between 2 and 3%.

### Model Description

The present test involved testing three different fuselages of identical planform in conjunction with a 55-deg cropped delta wing. Of the three fuselages, two had chine-shaped cross sections, while the third had a circular cross section. The planform and dimensions common to all three combinations are shown in Fig. 2. The wing was constructed of 0.050-in. aluminum sheet and was mounted either at the chine line or the center of the circular section. Orifices were installed in both the bottom and top surfaces of the fuselages, as well as near the leading edge of the wing. To avoid unwanted flow features associated with a transition from the forebody to an alternate aft-body cross section, each fuselage was manufactured with a constant cross section. Of course, only the fuselage forebody was exposed to the flow and generated the vortex system that would interact with the wing vortex system.

The two chine cross sections are shown in Fig. 3 and scale with the fuselage width. The chine shown in Fig. 3a is called the 7.5-deg chine because the total included angle at the chine line is 7.5 deg (the upper surface makes an angle of 5 deg to the plane of the wing, while the bottom makes an angle of 2.5 deg). The chine shown in Fig. 3b is the 90-deg chine because its total angle is 90 deg, 60 deg from the upper surface angle and 30 deg from the lower surface angle. Coordinates for the cross sections of both chines are given in Table 1.

The 7.5-deg chine cross section was chosen to be representative of a "sharp" chine edge, while the 90-deg chine was to represent a more moderate design. The circular cross section was selected as a baseline configuration to which comparisons can be made.

### Data Acquisition and Procedure

Videotape as well as 35-mm slide film was used during the test program. Since the vortex-burst locations, which are the emphasis of this report, were found to be somewhat unsteady during the tests, the videotape record was used as the most ac-

Presented as Paper 86-1835 at the AIAA 4th Applied Aerodynamics Conference, San Diego, CA, June 9-11, 1986; received Aug. 5, 1986; revision received April 17, 1987. 

*Research Scientist. Associate Fellow AIAA.

Table 1 Coordinates of chine cross sections[a]

| | 90-deg chine | | 7.5-deg chine | |
|---|---|---|---|---|
| $Y$ | $Z_{upper}$ | $Z_{lower}$ | $Z_{upper}$ | $Z_{lower}$ |
| 0 | 1.000 | −0.500 | 1.000 | −0.500 |
| 0.1 | 0.991 | −0.488 | 0.950 | −0.475 |
| 0.2 | 0.963 | −0.458 | 0.826 | −0.413 |
| 0.3 | 0.914 | −0.413 | 0.665 | −0.332 |
| 0.4 | 0.841 | −0.360 | 0.494 | −0.247 |
| 0.5 | 0.746 | −0.301 | 0.334 | −0.167 |
| 0.6 | 0.628 | −0.239 | 0.202 | −0.101 |
| 0.7 | 0.491 | −0.178 | 0.104 | −0.052 |
| 0.8 | 0.338 | −0.117 | 0.043 | −0.021 |
| 0.9 | 0.172 | −0.058 | 0.012 | −0.006 |
| 1.0 | 0. | 0. | 0. | 0. |

[a]See Fig. 3 for coordinate definition.

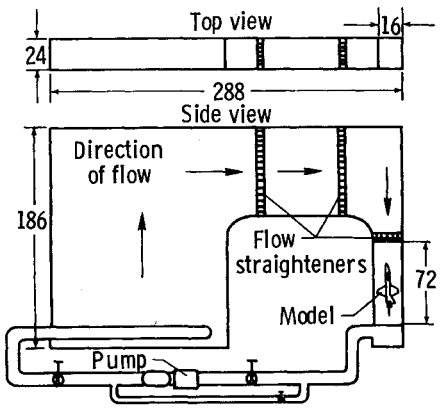


Fig. 1 Ames-Dryden water tunnel (dimensions in inches).

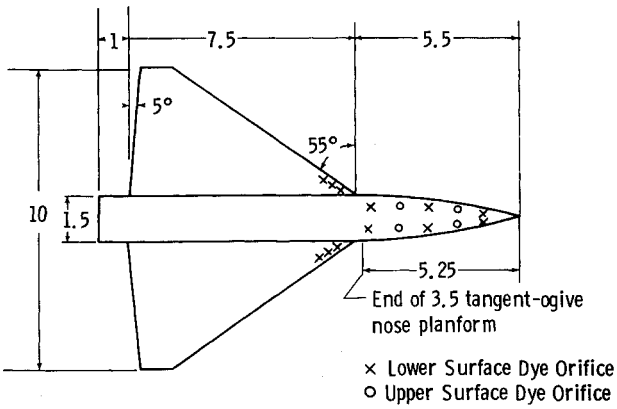


Fig. 2 Planform dimensions (in.) common to all three configurations.

curate and easiest means of determining vortex-burst locations. Measurements of burst locations were facilitated by a 1-in. grid laid out on the wing. Representative 35-mm photographs, though not always as accurate in depicting burst as the videotape, are included to illustrate the flow patterns generated by these three fuselage/wing configurations at various angles of attack $\alpha$ and sideslip $\beta$.

The main-wing vortex-burst locations will be given in terms of longitudinal position along the fuselage $x$, as measured from the trailing-edge/fuselage junction in percent of the wing chord $c$ along the fuselage. A value of zero represents burst even with the trailing-edge junction, while a value of 100% represents bursting at the wing leading-edge/fuselage junction. The repeatability of burst locations between different runs normally fell within $\pm 0.50$ in. or $\pm 7\%$ of $c$.

Photographs were taken at test $\alpha$ of 0, 10, 15, 17.5, 20, 22.5, 25, 30, 35, 40, 45, and 50 deg. The inclusion of all these

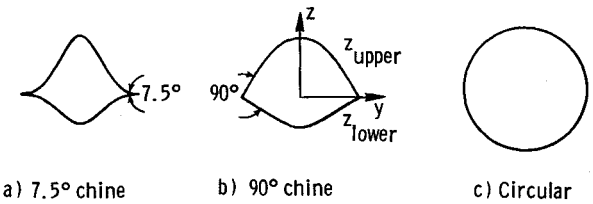


Fig. 3 Fuselage cross sections.

records into this paper is not possible. The reader is, however, referred to Ref. 8 for a more complete photographic record of this water-tunnel test. Furthermore, photographs and burst data are shown herein only for $\alpha \geq 15$ deg since the flow pictures and vortex burst behavior for $\alpha < 15$ deg can be misleading at low Reynolds numbers. A report by Erickson[9] has a more complete discussion of this issue.

## Results and Discussion

The photographs and summaries of vortex burst data for all three forebody/wing configurations will be grouped by value of sideslip, either 0 or 5 deg. For $\beta = 0$ deg, the summary vortex burst plot will follow representative photographs for all the configurations, but for $\beta = 5$ deg, a summary plot will follow each set of configuration photographs. The circular configuration will then be used to address possible concerns that the present water-tunnel burst data may not be indicative of higher Reynolds number air data.

### $\beta = 0$ deg

Representative planview photographs for the 7.5-deg chine, 90-deg chine, and circular forebody configurations are shown in Figs. 4–6, respectively. A summary plot of wing-vortex burst locations for all three configurations is given in Fig. 7.

The key features of the flow generated by the 7.5-deg chine forebody, as seen in the photographs of Figs. 4a–4e, are 1) a strong forebody vortex system interacting with the wing vortices, 2) a slowly progressing vortex-burst position over the wing that does not reach the leading-edge/fuselage junction until $\alpha = 45$ deg, and 3) symmetric flow patterns left to right even up to $\alpha = 50$ deg. Because of the persistence of relatively strong forebody vortices up to $\alpha = 50$ deg, long after one would normally consider the main wing to be substantially stalled, the aircraft designer needs to consider that the associated vortex lift induced on the forebody may lead to a pitchup problem. In fact, a pitchup problem has been documented by Erickson and Brandon[10] for a similar configuration, a chine-shaped forebody on a 60-deg delta wing.

The interaction between the forebody and main wing vortices for the more moderate 90-deg chine results in bursts occurring closer to the leading-edge/fuselage junction than for the 7.5-deg chine (see Fig. 7). This can be seen in the photographs by comparing Figs. 5a and 5b, which show this configuration at $\alpha = 15$ and 22.5 deg, to Figs. 4a and 4b for the 7.5-deg forebody configuration. While not as obvious in the still photographs as in the videotape record, the forebody vortices, as judged by helix angle, appear to be weaker for the 90-deg chine than for the 7.5-deg chine.

For the circular cross section, the forebody/wing vortex system is least able to resist wing vortex burst (see Fig.7). The forebody vortices, if they do exist, are now obviously weaker than for either chine as evidenced by the apparent lack of rollup of the forebody streamlines for $\alpha = 15$ deg (see Fig. 6a). The nature of the forebody streamlines and their interaction with the wing vortex is also changed. For both chines, the forebody streamlines, which were in obvious vortical flowfields, wrapped around the main wing vortex before going 2.5 in. over the wing. For the circular case, the forebody streamlines are spread into a sheet-like structure and are entrained into the main wing vortex over the entire wing.

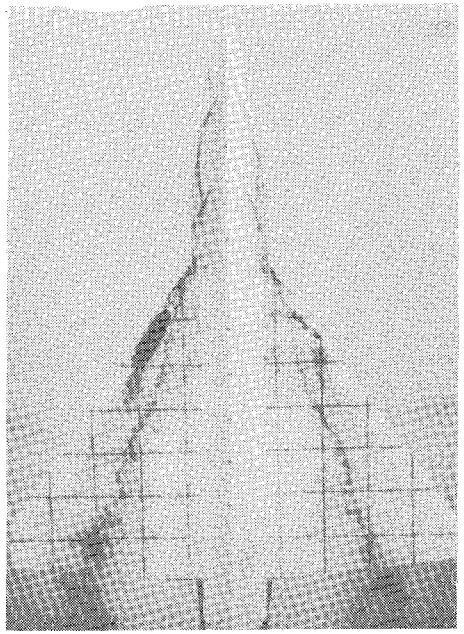

a) $\alpha = 15$ deg.

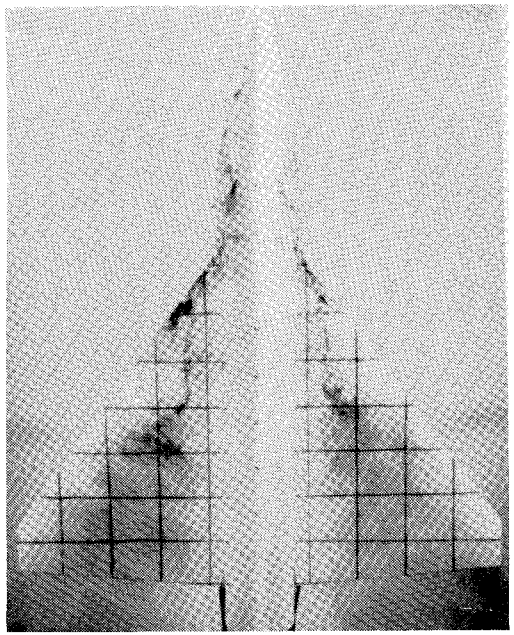

b) $\alpha = 22.5$ deg.

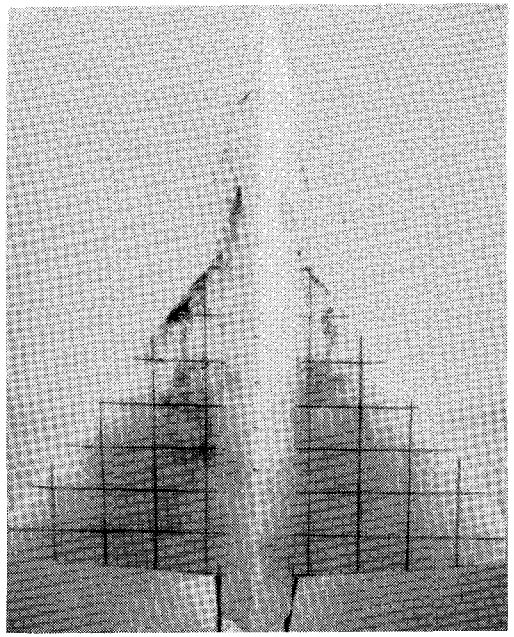

c) $\alpha = 30$ deg.

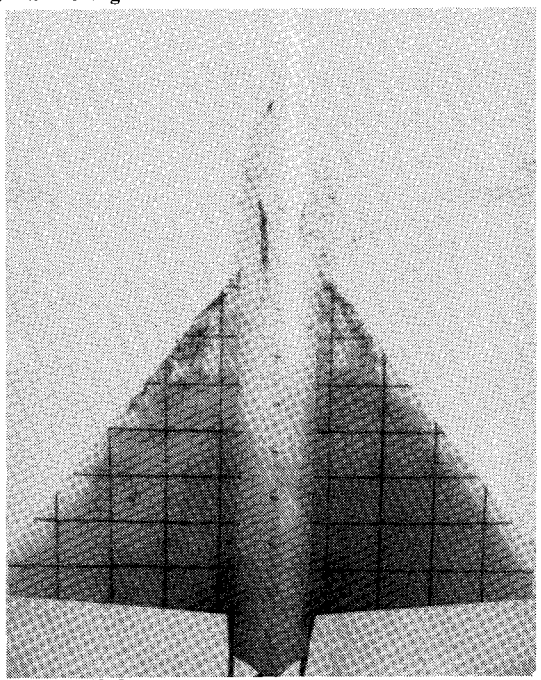

d) $\alpha = 40$ deg.

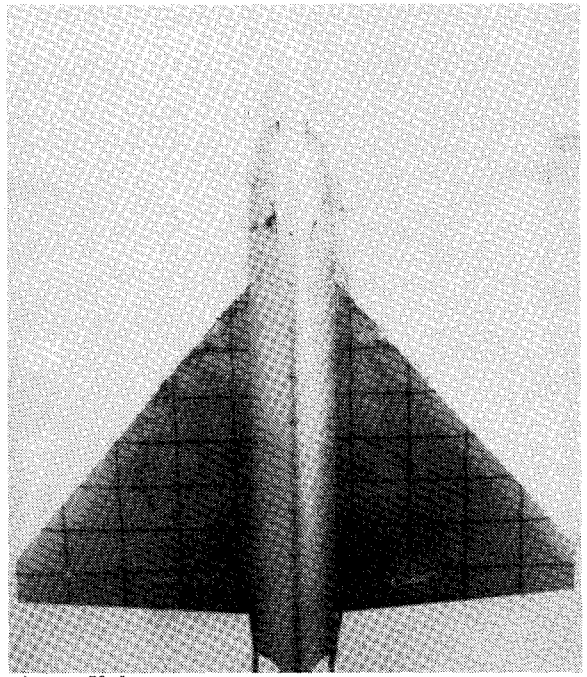

e) $\alpha = 50$ deg.

Fig. 4 7.5-deg chine configuration, $\beta = 0$ deg.

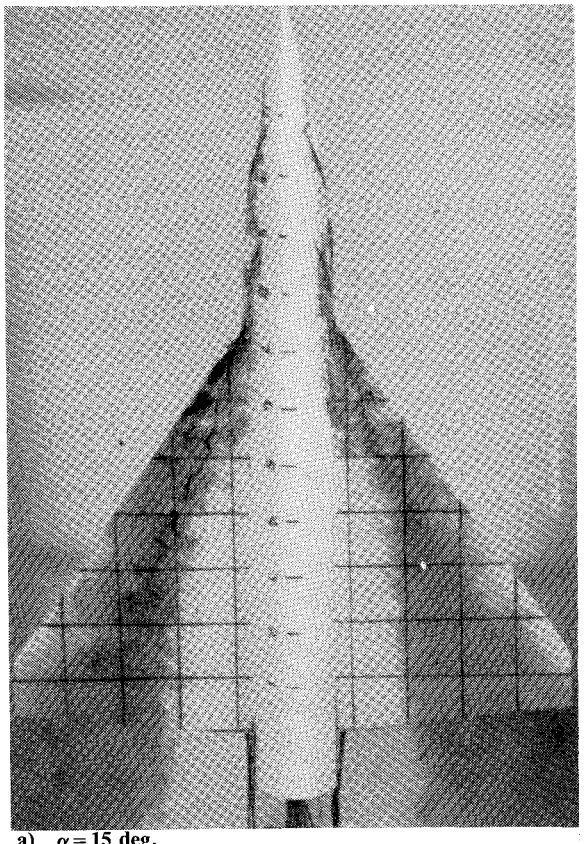

a) $\alpha = 15$ deg.

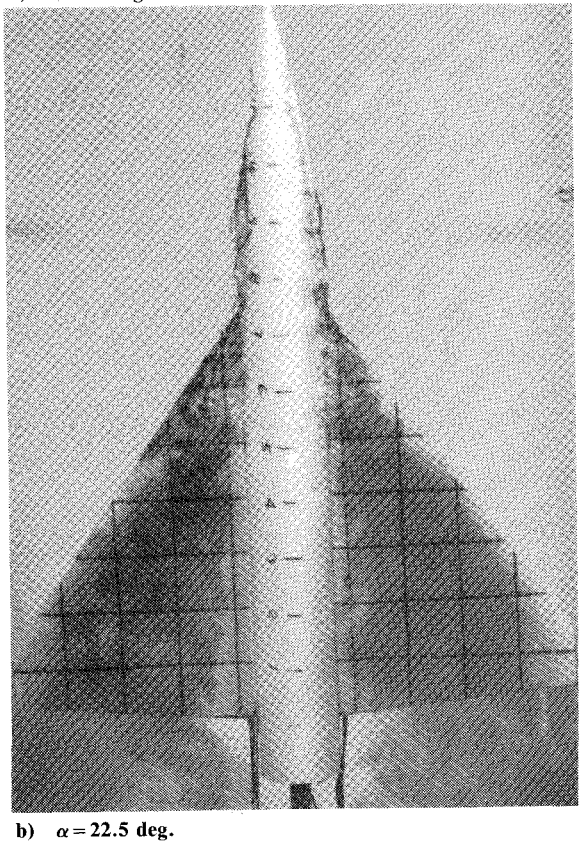

b) $\alpha = 22.5$ deg.

**Fig. 5 90-deg chine configuration, $\beta = 0$ deg.**

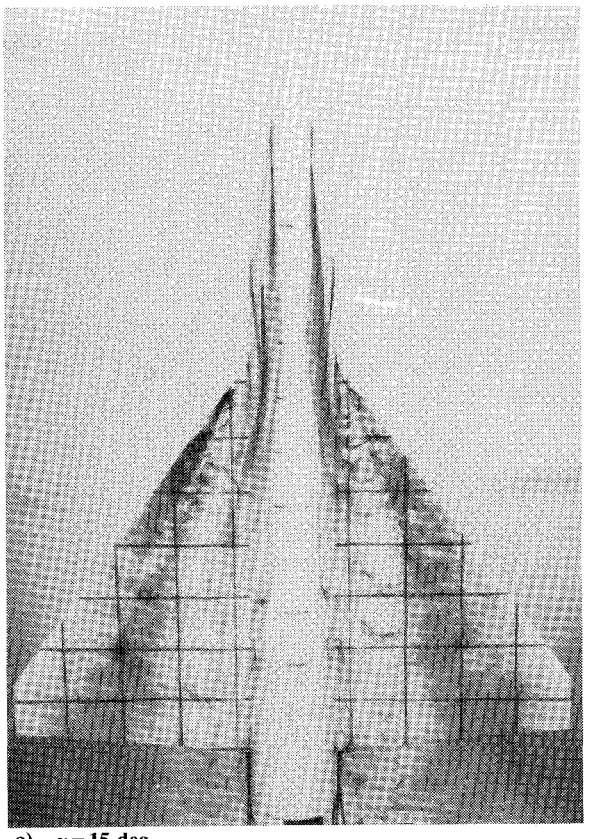

a) $\alpha = 15$ deg.

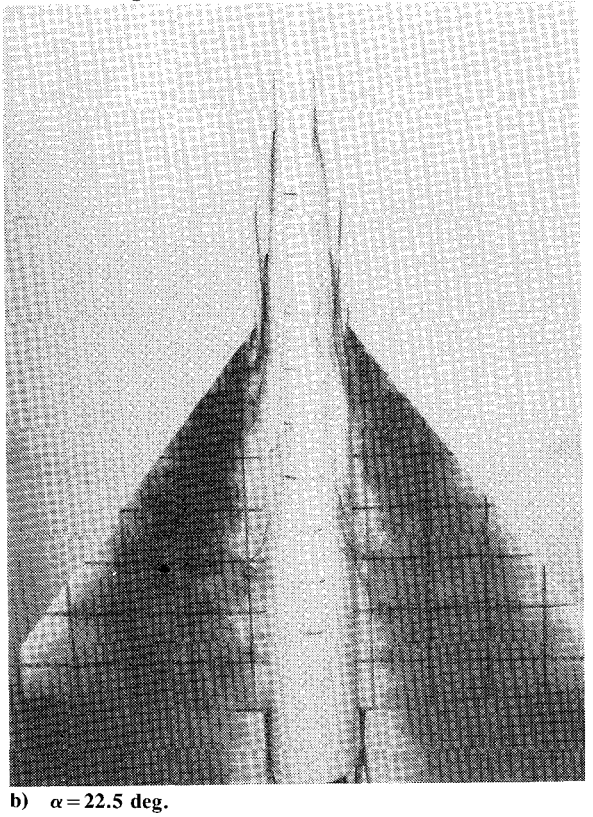

b) $\alpha = 22.5$ deg.

**Fig. 6 Circular fuselage configuration, $\beta = 0$ deg.**

In the vortex-burst summary plot, Fig. 7, the 7.5-deg chine is more effective in delaying wing vortex burst than the 90-deg chine when compared to the circular baseline. In the range of $\alpha = 20$ deg, the 7.5-deg chine delays burst by about 40% of the chord when compared to the circular configuration, while the 90-deg chine delays burst by about 20%. This effectiveness of the 7.5-deg chine is evidently due to its sharper chine angle generating forebody vortices that interact more favorably with the main wing vortices. As mentioned earlier, the 7.5-deg chine appears to develop stronger forebody vortices, which may explain its greater effectiveness.

That the 7.5-deg chine should generate stronger forebody vortices than the other bodies is not surprising and can be explained by looking at the fuselage cross sections in Fig. 3. In

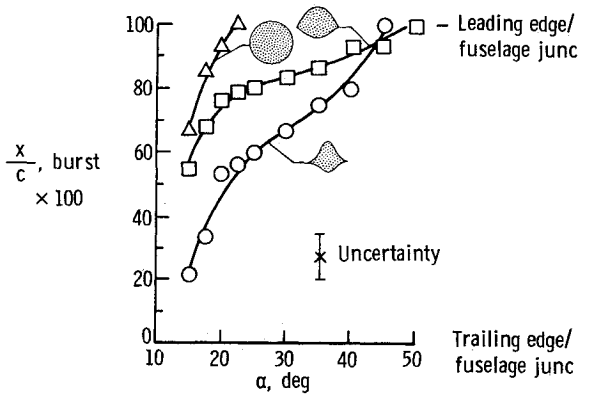


**Fig. 7 Wing vortex-burst locations, all configurations, $\beta = 0$ deg. Data symbols represent averages of left and right wing panels.**

the progression from circular to 90-deg chine to 7.5-deg chine, there is no discontinuity for the smooth side in the circular case, a 90-deg slope discontinuity for the 90-deg chine, and a 172.5-deg slope discontinuity for the 7.5-deg chine. The stronger discontinuities in slope and the associated increases in singularity strength should lead to higher velocities approaching the point of separation and, consequently, stronger vorticity being shed at that point. (The relationship between velocity at the separation point and the resulting vorticity being shed is explained, for example, by Mendenhall.[11] He shows that the vorticity being generated by the boundary-layer separation is proportional to the velocity at separation squared.)

Also, in a relevant analysis of potential flow with shed vortices about a rhombic cone, Nutter[12] uses Smith's model[13] to examine the influence of the included side-edge wedge angle on the strength of the shed vorticity. Nutter's analysis reinforces the above reasoning with the chine angles because he found that his smaller included wedge angles at the sides of his rhombic cone (corresponding to the smaller chine angles) resulted in higher amounts of total circulation about his calculated vortices.

Assuming, therefore, that the 7.5-deg chine did indeed generate the greatest amount of forebody vorticity, its greater effectiveness in delaying wing vortex burst is similar to the results of a study by Frink and Lamar.[14] Their study involved water-tunnel tests of a fuselage/strake/trapezoidal wing configuration. The authors found that for fixed-shape strakes of different size, the larger strakes with their greater amount of vorticity delayed burst over the wing more effectively.

### $\beta = 5$ deg

Representative photographs and vortex-burst summaries for the configurations are shown in Figs. 8–13. In two of the summary plots, the vortex burst locations for $\beta = 0$ deg are given for purposes of comparison.

Flow asymmetries appear in sideslip for all the configurations; however, they are the greatest for the 7.5-deg chine (compare Figs. 9, 11, and 13). An interesting feature of the flow on the leeward sides of both chine configurations is that the leeward forebody and wing vortices appear to interact less strongly because the vortices travel further before coalescing when compared to either the windward sides or the $\beta = 0$ deg cases. At the same time, however, vortex burst is delayed on the leeward side. The windward forebody and wing vortices are marked by strong interaction and relatively early burst when compared to $\beta = 0$-deg data.

Figures 8a and 8b illustrate these trends for the 7.5-deg chine at $\alpha = 15$ and 22.5 deg. The summary plot for the 7.5-deg chine configuration at $\beta = 5$ deg is shown in Fig. 9. Comparing the burst locations for $\beta = 5$ and 0 deg, it is seen that throughout the $\alpha$ range the burst on the windward side moves toward the leading-edge/fuselage junction, while the burst on the leeward sides moves rearward. The large differences in burst location could cause concern for possibly unstable values of rolling moment. While the force data published by Erickson and Brandon[10] did not find large unstable rolling moments for their configuration without a vertical tail, this problem of differences in burst locations during sideslip should be scrutinized for each new chine configuration.

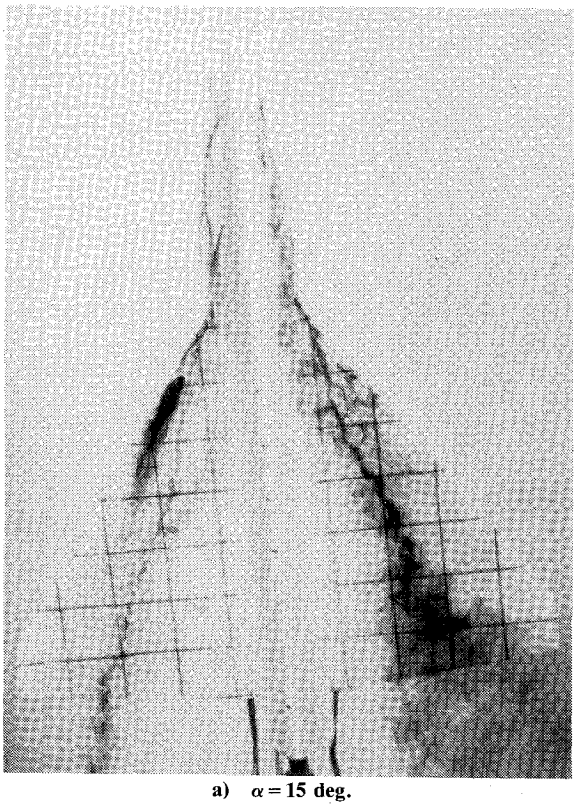

a) $\alpha = 15$ deg.

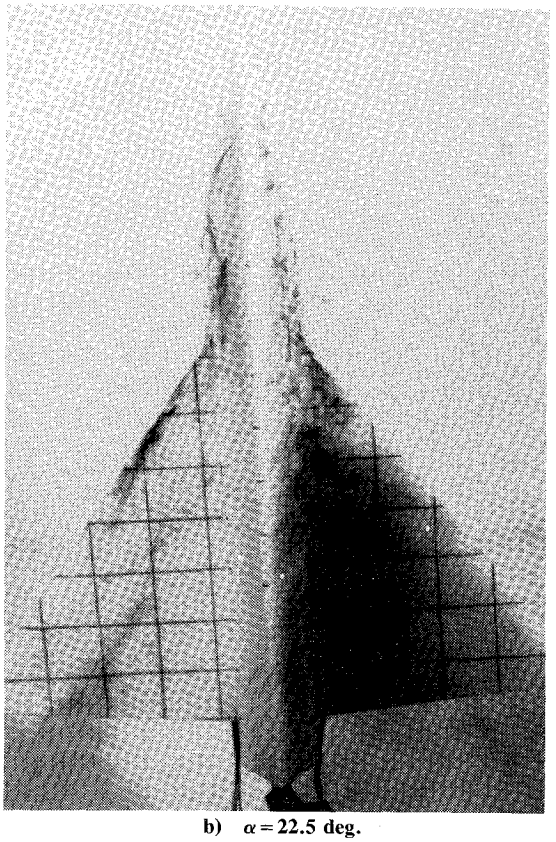

b) $\alpha = 22.5$ deg.

**Fig. 8 7.5-deg chine configuration, $\beta = 5$ deg.**

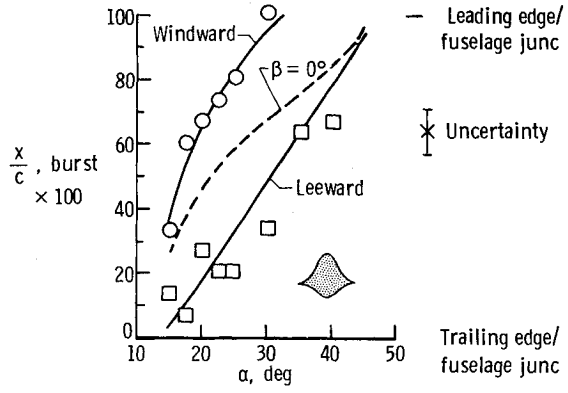


**Fig. 9 Wing vortex-burst locations, 7.5-deg chine configuration, $\beta = 5$ deg. Line for $\beta = 0$-deg burst shown for comparison.**

The 90-deg chine photographs are shown in Figs. 10a and 10b. Comparing Fig. 10a for $\alpha = 15$ deg to Fig. 5a for $\beta = 0$ deg, one can again see burst locations moving toward the trailing edge on the leeward side and the leading edge on the windward side. Also, the upper forebody dye lines on the windward side are not entrained into the windward forebody vortex, which suggests that the windward forebody vortex is either moving downward toward the plane of the wing and/or weakening. (Side views of the windward side were not available for analysis.) When $\alpha$ is increased to 22.5 deg (Fig. 10b), the windward forebody vortex is strong enough to entrain the dye emanating from the upper dye ports. In contrast to the 7.5-deg chine at $\alpha = 22.5$ deg and $\beta = 5$ deg, the stalled windward wing flow is crossing the fuselage to the leeward side. The summary burst plot is shown in Fig. 11. As in the case of the 7.5-deg chine forebody, the 90-deg chine experiences large differences in burst location between the windward and leeward panels.

The corresponding sideslip photographs for the circular cross section are shown in Figs. 12a and 12b, which show not only the relatively weak interaction between the forebody and wing vortices, but also the small influence that sideslip has on burst location (see Fig. 13). The relative insensitivity to sideslip may be due to the presence of the fuselage, which can reduce the effective sideslip seen by the wing, as explained by Polhamus and Sleeman.[15] This reduction in effective sideslip is due to alignment of the flow along the fuselage and should be most important for the circular body because its relative volume (1.00) is greater than that of either the 90-deg body (0.60) or 7.5-deg body (0.39) and the burst points are occurring relatively close to the leading-edge/fuselage junction.

### Comparison of Vortex Burst Points to Air Data

In order to address possible concerns that the present water-tunnel data at low Reynolds number may not be representative of higher Reynolds number air results, the air data of Wentz and Kohlman[16] were chosen for comparison. Of the three bodies tested, the circular body should be most representative of vortex burst over a simple 55-deg delta wing without a fuselage because of its relatively weak forebody vortices. Figure 14a compares the burst locations and, in fact, shows that burst at a given chord location for the Wentz and Kohlman data occurred at angles of attack roughly 4 deg higher than those for the water tunnel. However, there are at least three differences between the tests that may explain these differences in burst location. They are the presence of the fuselage, the high blockage ratio in the water tunnel, and the differences in Reynolds number.

The first difference can occur because the presence of the fuselage itself changes the effective angle of attack of the main wing due to the upwash associated with flow around the fuselage. This effective $\alpha$ concept is explained by Hemsch and Nielsen[17] and is related to experimental $\alpha$ by the relation

$$\tan\alpha_{\text{eff}} = K_W \tan\alpha \qquad (1)$$

where $K_W$ is the slender-body-theory interference factor associated with fuselage upwash.[18] A value of $K_W = 1.118$ is

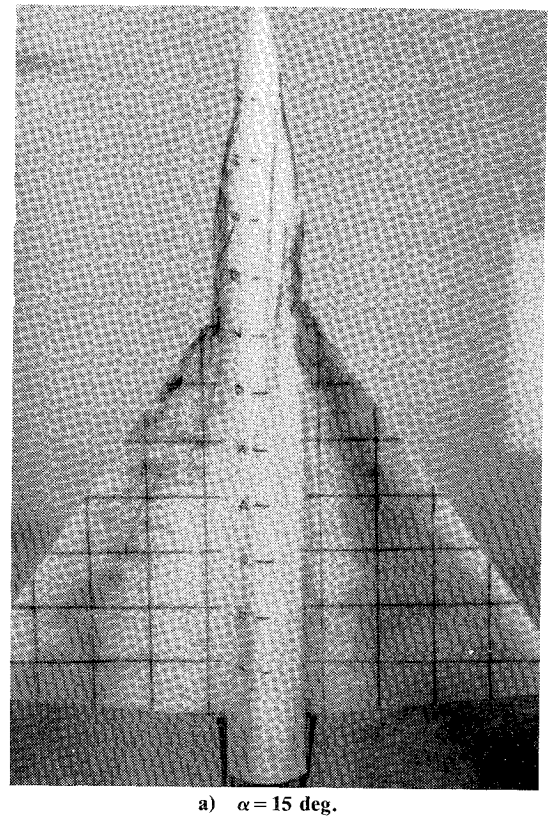

a) $\alpha = 15$ deg.

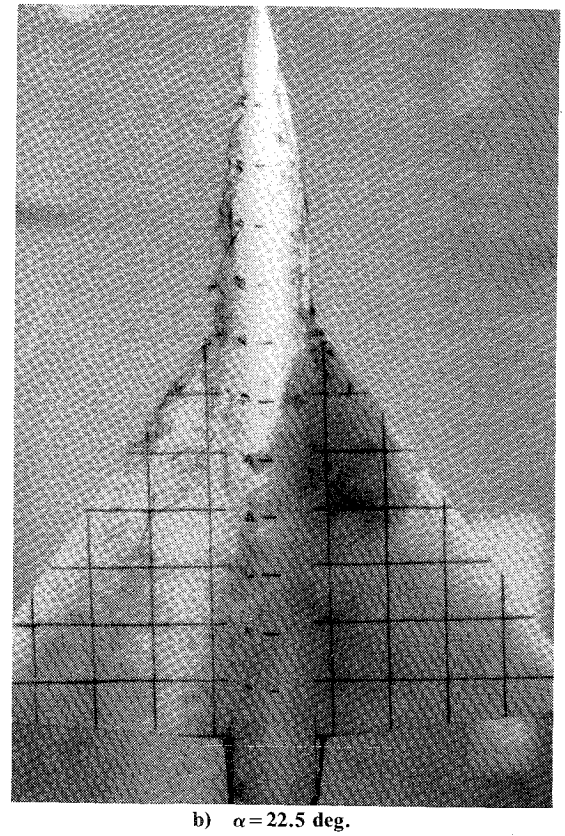

b) $\alpha = 22.5$ deg.

**Fig. 10 90-deg chine configuration, $\beta = 5$ deg.**

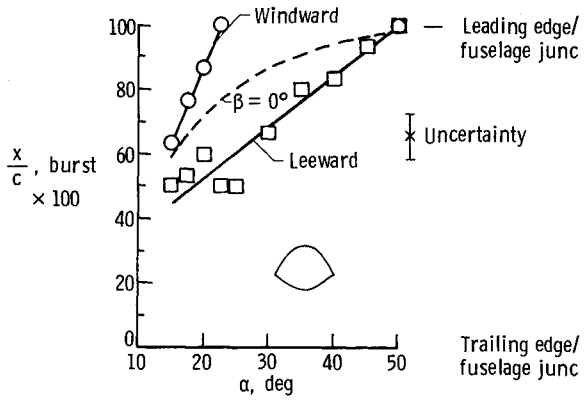


**Fig. 11 Wing vortex-burst location, 90-deg chine configuration, $\beta = 5$ deg. Line for $\beta = 0$-deg burst shown for comparison.**

determined from Ref. 18 using the ratio of the maximum wingspan (10 in.) divided by the fuselage width (1.5 in.). When plotting burst points in Fig. 14b as a function of $\alpha$ as corrected by Eq. (1), it is seen that the agreement between Wentz and Kohlman and the present data are improved.

The second difference between the present data and the Wentz and Kohlman data occurs because of the large differences in relative model-to-tunnel size between the two experiments. For the water-tunnel tests, the model wingspan-to-tunnel width ratio is 0.63 (typical for water-tunnel studies), while the Wentz and Kohlman ratio is only 0.21. Calculating approximate corrections to $\alpha$ due to the presence of the sidewalls by using Ref. 19, this second correction brings the data even closer together (see Fig. 14c).

The third difference between the data sets is in Reynolds number. The water- and wind-tunnel Reynolds numbers based on wing-root chord are, respectively, $1.4 \times 10^4$ and $0.6 \times 10^6$. The questions of burst differences between a water-tunnel study at low Reynolds numbers and a wind-tunnel study at higher Reynolds numbers have been addressed by Lamar and Frink[20] for a fuselage-strake-trapezoidal wing configuration. They point out that while caution is in order, water-tunnel trends can qualitatively be quite helpful. The good agreement between the corrected circular fuselage data and the Wentz and Kohlman data suggests that Reynolds number effects are minimal for the circular fuselage case. Effects of Reynolds number on fuselage separation should be less for the two chine fuselages, at least for $\beta = 0$ deg and $\alpha \geq 20$ deg, because their sharp edges will fix the fuselage separation line. It remains to be seen if higher Reynolds numbers will influence the vortex burst locations for the chined configurations through turbulent separation on the wing planform or through effects on the vortex core. The general trend, however, for the sharper chine edges to generate stronger vortices that interact with the wing vortices and delay vortex bursting, should be the same, independent of Reynolds numbers.

## Summary of Results

It has been shown in this report that the 7.5- and 90-deg chine-shaped forebodies can delay wing vortex-burst location significantly when compared to a circular section forebody that served as a baseline configuration. Summary plots of vortex-burst location are presented that detail the $\alpha$ and $\beta$ dependence of burst for each configuration and permit configuration-to-configuration comparisons.

The 7.5-deg chine section is found to be more effective than the 90-deg chine in delaying vortex burst. In zero sideslip, the 7.5-deg chine configuration appears to have symmetric flow from left to right but could experience a pitchup problem at high $\alpha$. In sideslip, however, large differences between windward and leeward vortex-burst locations occur for the 7.5-deg chine and, to a lesser extent, for the 90-deg chine. This may serve as a warning that unstable rolling moments are a possibility with this class of forebodies.

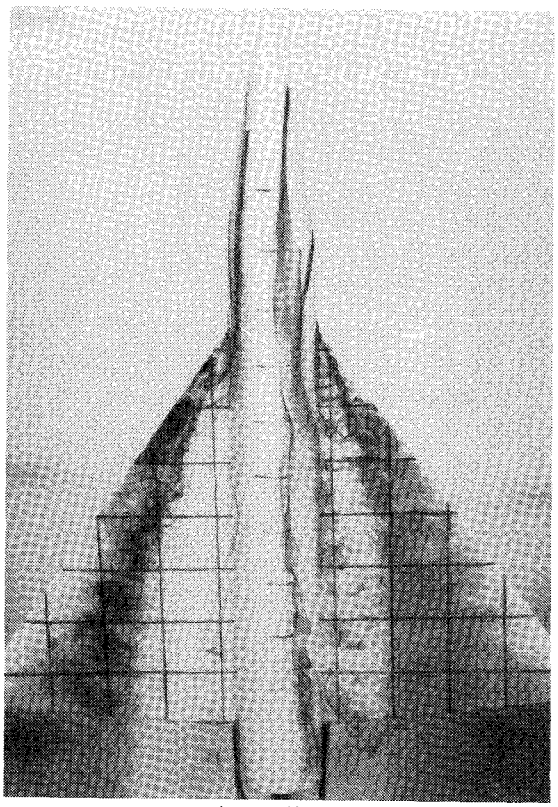

a) $\alpha = 15$ deg.

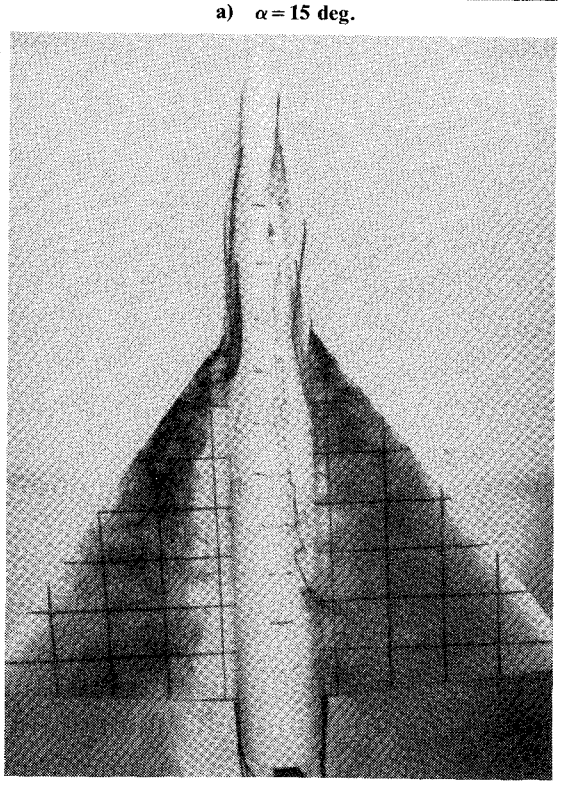

b) $\alpha = 22.5$ deg.

**Fig. 12 Circular fuselage configuration, $\beta = 5$ deg.**

Finally, to address concerns that this water-tunnel study may not be representative of higher Reynolds number air data, the $\alpha$ dependence of the circular-section burst data is corrected for influences of fuselage upwash and sidewall interference. The circular burst data are then shown to be in good agreement with air data for a simple 55-deg delta wing taken by Wentz and Kohlman.

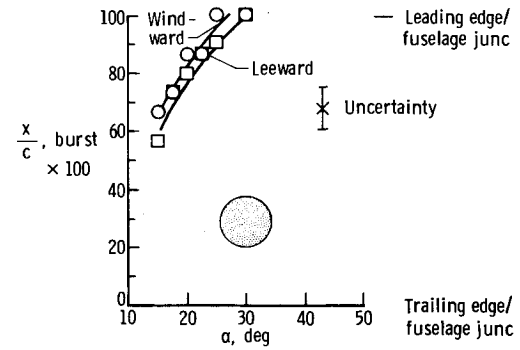


**Fig. 13 Wing vortex-burst locations, circular fuselage configuration, $\beta = 5$ deg.**

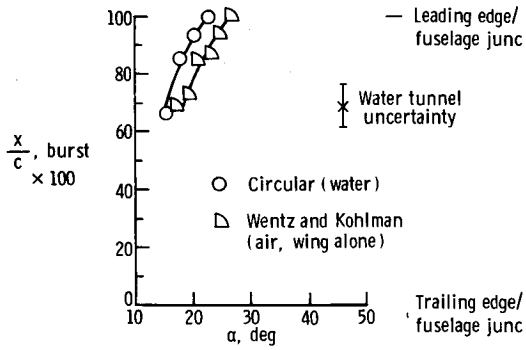


**a) Uncorrected.**

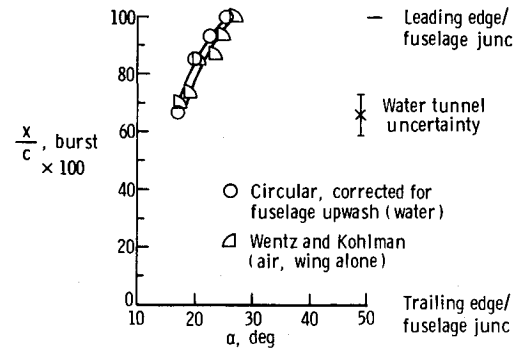


**b) Corrected as indicated.**

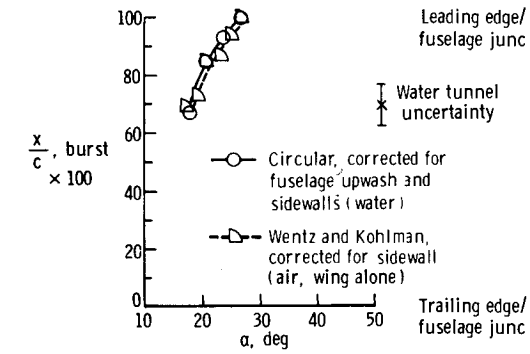


**c) Corrected as indicated.**

**Fig. 14 Water and air vortex-burst locations compared (Wentz and Kohlman data from Ref. 16).**

## Acknowledgments

The data used in preparing this report were gathered while the author was serving as a reservist in the United States Air Force, assigned to AFWAL/FIMM, Wright-Patterson Air Force Base, Ohio.

## References

[1]Herbst, W.B., "Future Fighter Technologies," *Journal of Aircraft*, Vol. 17, Aug. 1980, pp. 561–566.

[2]Skow, A.M. and Erickson, G.E., "Modern Fighter Aircraft Design for High Angle-of-Attack Maneuvering," AGARD-LS-121, Dec. 1982, Paper 4.

[3]Gallaway, C.R., "Aeromechanic Discussions of Supermaneuverability," AFWAL-TM-85-211, April 1985.

[4]Hunt, B.L., "Asymmetric Vortex Forces and Wakes," AIAA Paper 82-1336, Aug. 1982.

[5]Ericsson, L.E. and Reding, J.P, "Asymmetric Vortex Shedding from Bodies of Revolution," *Progress in Astronautics and Aeronautics*: *Tactical Missile Aerodynamics,* edited by M.J. Hemsch and J.N. Nielsen, Vol. 104, AIAA, New York, 1986.

[6]Polhamus, E.C., "A Review of Some Reynolds Number Effects Related to Bodies at High Angles of Attack," NASA CR-3809, Aug. 1984.

[7]Lamont, P.J., "The Effect of Reynolds Number on Normal and Side Forces on Ogive-Cylinders at High Incidence," AIAA Paper 85-1799, Aug. 1985.

[8]Hall, R.M. and Del Frate, J.H., "Interaction Between Forebody and Wing Vortices—A Water Tunnel Study," AFWAL-TM-85-252, Jan. 1986.

[9]Erickson, G.E., "Vortex Flow Correlation," ICAS Paper 82-6.6.1, Aug. 1982.

[10]Erickson, G.E. and Brandon, J.M., "Low-Speed Experimental Study of the Vortex Flow Effects of a Fighter Forebody Having Conventional Cross-Section," AIAA Paper 85-1798, Aug. 1985.

[11]Mendenhall, M.R., Spangler, S.B., and Perkins, S.C. Jr., "Vortex Shedding from Circular and Noncircular Bodies at High Angles of Attack," AIAA Paper 79-0026, Jan. 1979.

[12]Nutter, J., "Leading-Edge Separation from a Thick, Conical, Slender Wing at Small Angles of Incidence," *Journal of Engineering Mathematics,* Vol. 15, April 1981, pp. 103–117.

[13]Smith, J.H.B., "Improved Calculations of Leading-Edge Separation from Slender Delta Wings," RAE TR 66070, 1966.

[14]Frink, N.T. and Lamar, J.E., "Water-Tunnel and Analytical Investigation of the Effect of Strake Design Variables on Strake Vortex Breakdown Characteristics," NASA TP-1676, 1980.

[15]Polhamus, E.C. and Sleeman, W.C. Jr., "The Rolling Moment Due to Sideslip of Swept Wings at Subsonic and Transonic Speeds," NASA TN D-209, 1960.

[16]Wentz, W.H. Jr. and Kohlman, D.L., "Wind Tunnel Investigations of Vortex Breakdown on Slender Sharp-Edged Wings," NASA CR-98737, Nov. 1968.

[17]Hemsch, M.J. and Nielsen, J.N., "Equivalent Angle-of-Attack Method for Estimating Nonlinear Aerodynamics of Missile Fins," *Journal of Spacecraft,* Vol. 20, July–Aug., 1983, pp. 356–362.

[18]Nielsen, J.N., *Missile Aerodynamics,* McGraw-Hill, New York, 1960.

[19]Sanders, J. and Pounder, J.R., "Wall Interference in Wind Tunnels of Closed Rectangular Section," National Research Council of Canada, AR-7, 1949.

[20]Lamar, J.E. and Frink, N.T., "Experimental Analytical Study of the Longitudinal Aerodynamic Characteristics of Analytically and Empirically Designed Strake-Wing Configurations at Subcritical Speeds," NASA TP-1803, 1981.